A dc-Side Sensorless Cascaded H-Bridge Multilevel Converter Based Photovoltaic System

G. Farivar, *Student Member, IEEE*, B. Hredzak, *Senior Member, IEEE*, V. G. Agelidis, *Fellow, IEEE*

***Abstract*—In this paper a cascaded H-Bridge (CHB) multilevel converter based Photovoltaic (PV) system with no voltage or current sensors at the dc-side is proposed. Eliminating the dc-side sensors simplifies the hardware, leading to lower cost and higher reliability of the PV system. A novel scheme estimating the capacitors' voltages from the output ac voltage of the inverter is developed. The scheme allows replacing all dc-side voltage sensors by a single voltage sensor at the ac-side of the converter. Furthermore, the dc current sensors, conventionally required for the maximum power tracking (MPPT), are also eliminated. Instead, the outputs from the capacitors' voltage control systems are utilized for the MPPT. The effectiveness of the proposed dc-side sensorless system is experimentally demonstrated on a 2 kW single-phase 7-level CHB converter based PV system.**

***Index Terms*— Cascaded H-bridge converter, capacitor voltage estimation, photovoltaic system**

I. Introduction

APPLICATION of the cascaded H-bridge multilevel converters (CHB-MCs) in Photovoltaic (PV) systems has been investigated in many technical papers [1]-[17]. However, none of these studies have focused on simplifying the system hardware by reducing the sensor count.

Reducing the sensor count is of great importance because having both the dc voltage and the dc current sensors for each H-bridge cell increases the system cost and complexity and also reduces its reliability. Furthermore, extending the capacity of an existing system by adding more cells becomes difficult due to additional wirings required for the sensors and a potentially limited number of I/O channels available on the central control board. Therefore, eliminating either or both the dc current or voltage sensors is beneficial.

In a conventional PV system, both the dc current and voltage sensors are required by the Maximum Power Point Tracking (MPPT) algorithm. Several single voltage sensor PV systems were proposed in literature [18]-[21]. In [18], the dc voltage sensor was eliminated and the MPPT was implemented using the dc-dc converter's duty cycle and the dc current measurement. In [19], the MPPT was implemented by only sensing the dc voltage. The change in the power delivered by the inverter was inferred from the control signals. Tracking the actual maximum power point of a PV array using only the voltage sensor was performed by connecting a capacitive load to it in [20], [21]. However, a specific type of converter was required to implement the proposed technique. In summary, none of these studies were implemented for a CHB-MC based PV system and in none of them were both the DC current and the dc voltage sensors eliminated.

In conventional CHB-MC based PV systems the dc current sensors are required by the MPPT module and the dc voltage sensors are required for the capacitors' voltages control system and the Pulse Width Modulation (PWM) generator. Hence, in higher level converters, many isolated dc sensors are required, which increases the system cost and complexity. The dc voltage sensors elimination in CHB-MCs was addressed in a few papers, but only for STATCOMs. The dc voltage sensors were replaced by a single sensor at the AC side of the CHB inverter-based STATCOM in [22]. The voltage measurement for each cell was performed at a specific moment of switching in which the output of all cells except one was zero. Therefore, the sampling frequency of capacitors' voltages measurement was low and varying, which is not desirable. This drawback was addressed in [23], where the sampling frequency was kept constant at twice the switching frequency. However, no experimental validation was provided. In [24], the capacitor voltage sensors were replaced by an observer in the CHB based STATCOM. However, the slow dynamics of the observer makes this method not suitable to perform the PWM switching or fast voltage control.

In this paper, for the first time, a dc-side sensorless CHB-MC based PV system which does not require any dc current or dc voltage sensors is proposed.

The rest of this paper is organized as follows: the proposed dc-side sensorless CHB-MC based PV system is introduced in Section II. The proposed single voltage sensor technique for measurement of capacitors' voltages is introduced in Section III. The voltage controller module, the MPPT module, the current controller module, the power sharing module and the switching module are described in Section IV. The simulation and experimental results are provided in Sections V and VI. Finally, conclusions are summarized in Section VII.

Manuscript received May 18, 2015; revised November 13, 2015 and January 5, 2016; accepted February 16, 2016.

The authors are with the Australian Energy Research Institute, School of Electrical Engineering and Telecommunications, University of New South Wales, Sydney, NSW 2052, Australia (e-mail: g.farivar@unsw.edu.au; b.hredzak@unsw.edu.au; vassilios.agelidis@unsw.edu.au).

This article has been accepted for publication in a future issue of this journal, but has not been fully edited. Content may change prior to final publication. Citation information: DOI 10.1109/TIE.2016.2544243, IEEE Transactions on Industrial Electronics

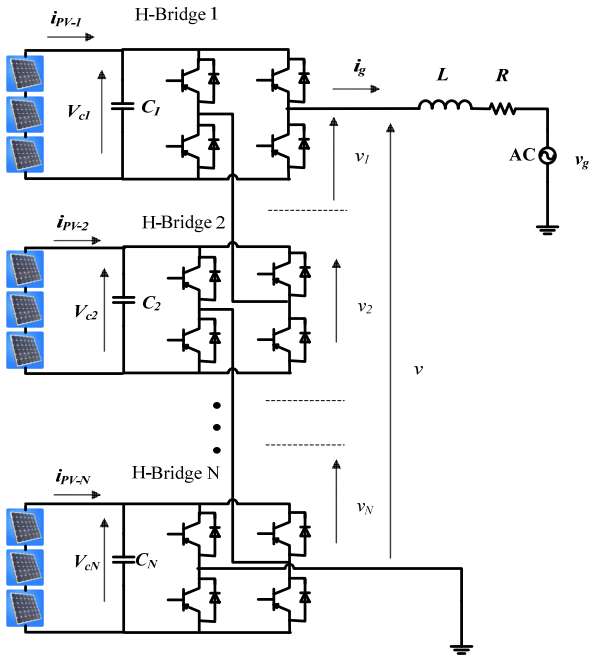

Fig. 1. CHB multilevel converter PV system

II. DC-Side Sensorless CHB Multilevel Converter Based PV Control System

Since the output voltage of the PV modules can vary in a wide range due to partial shading, the PV modules are traditionally connected to a fixed dc link voltage of the inverter via a dc-dc converter. However, by introducing the DC-DC converter the overall efficiency of this configuration is reduced by 4-10% [25] and the cost and complexity of the system is increased. However, since the CHB-MC allows controlling the individual capacitors' voltages independently, the PV modules can be connected directly to the dc links thus eliminating need for the dc-dc converters as shown in Fig. 1. Conventional control systems for this configuration require N H-bridges, N voltage sensors and N current sensors at the dc-side. In this paper, a dc-side sensorless control system for the configuration in Fig. 1 is proposed. The main advantage of the proposed control system, as compared to conventional ones, is that all dc-side current and voltage sensors are eliminated, which significantly reduces the system's complexity and cost. In the proposed control system, only one voltage sensor is required to measure the voltage at the ac-side of the CHB-MC. In addition, one voltage sensor is required to measure the grid voltage and one current sensor is required to measure the grid current.

Block diagram of the proposed control system is shown in Fig. 2. The ac output voltage v measured at the ac-side of the CHB-MC is used to estimate the capacitors' voltages in the Capacitors' Voltages Estimation Module (CVEM). The estimated capacitors' voltages are then used (i) as feedback signals in the voltage controller module, (ii) for feedforward compensation of the low order harmonic ripples in the switching module and (iii) to estimate the average PV modules' power in order to track the optimal operating point in the MPPT module. The measured grid voltage, v_g, and the grid current, i_g, are used by the current controller module. i_g is also used by the power sharing module to generate the voltage reference signals for the switching module. In the following sections, design and operation of each module is explained in detail.

III. Capacitors' Voltages Estimation Module

The capacitors voltages are estimated using a single voltage sensor which measures the ac output voltage, v, at the ac-side of the CHB-MC. This allows eliminating all dc-side voltage measurement sensors.

The measured ac output voltage, v, is sampled after each switching transition. Therefore, the voltage sampling frequency for each bridge is twice the switching frequency.
The ac output voltage, v, in an $(N+1)$-level CHB-MC is given by

$$v = \sum_{j=1}^{N} S_j V_{c-j} - DV_{diode} - MV_{switch} \quad (1)$$

where S_j=(0,+1,-1) is the switching function of the jth H-bridge, and V_{diode} and V_{switch} are the forward voltage drops across the conducting diode and switch, respectively. D and M represent the number of conducting diodes and switches, respectively, which can be calculated as [23]

$$\begin{aligned} D &= 2P + Z \\ M &= 2A + Z \end{aligned} \quad (2)$$

where P and A represent the number of H-bridges operating in the inverting and rectifying mode, respectively, and Z is the number of H-bridges generating zero voltage.

Then, the capacitor voltage V_{c-j} of the jth switched bridge can be determined from the measured ac output voltage, v, before and after each switching transition as [23]

$$V_{c-j} = \left| v' - v'' \right| \quad (3)$$

where v' is the AC output voltage measured before and v'' after the switching transition.

In Fig. 3, the voltage sampling instances for a 7-level CHB-MC (three H-bridges) are shown. As it can be seen, the sampling frequency is fixed at twice the switching frequency, which results in high resolution of the estimated capacitors' voltages.

The generated output ac voltage undergoes transients after each switching transition due to parasitic capacitances and inductances. Therefore, in order to allow sufficient time for the transients to decay and perform the measurement in the steady state, the measurement is performed after a time delay. However, when the pulse width is too narrow, there is not enough time to perform the estimation. In this case, the capacitors' voltages reconstruction mechanism disregards the narrow pulses, no estimation is performed, and previously reconstructed capacitors' voltages values are used. Similarly, when an H-bridge enters the over modulation region in which

This article has been accepted for publication in a future issue of this journal, but has not been fully edited. Content may change prior to final publication. Citation information: DOI 10.1109/TIE.2016.2544243, IEEE Transactions on Industrial Electronics

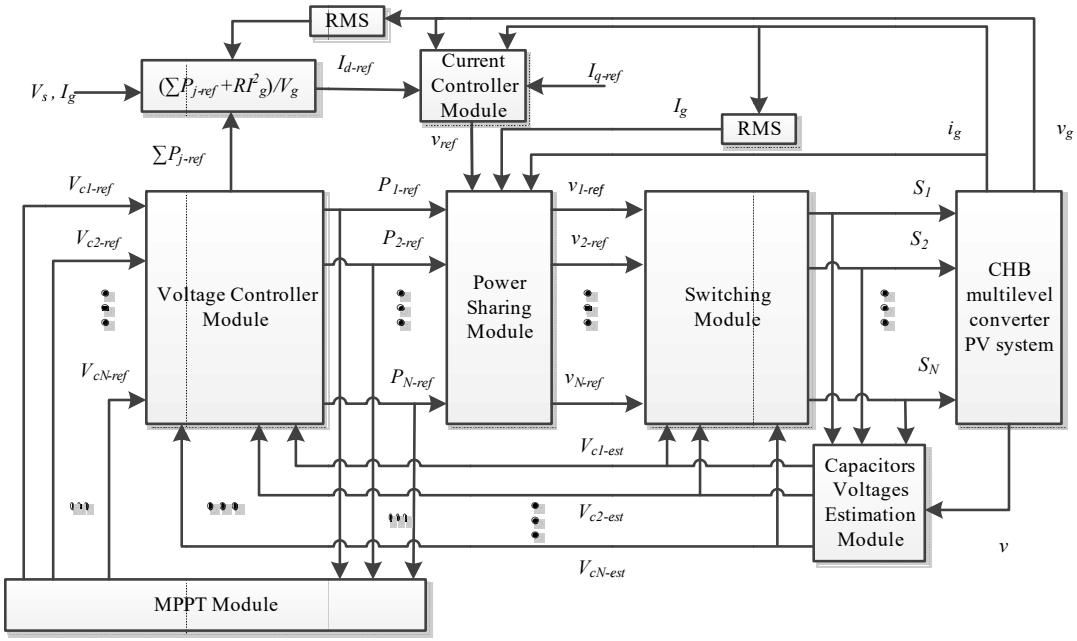

Fig. 2. Block diagram of the dc-side sensorless CHB multilevel converter based PV control system

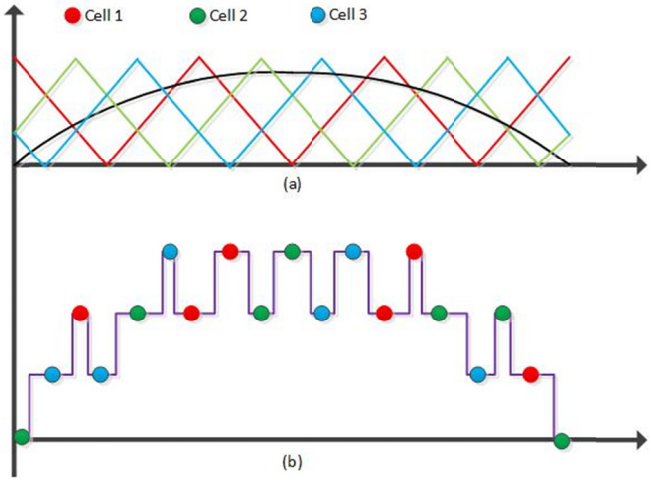

Fig. 3. (a): Reference voltage and carriers (b): Voltage estimation instances

no pulse occurs in the output voltage, the previously reconstructed capacitors' voltages values are used. Since the resolution of the proposed capacitors' voltages reconstruction method is high and the capacitors voltages cannot change abruptly, the assumption of using previously reconstructed capacitors' voltages does not deteriorate performance of the system.

IV. Other Modules

A. Voltage controller module and MPPT module

The voltage controller module and the MPPT module are shown in Figs. 4 and 5. The voltage controller module consists of the PI voltage controllers, which control each capacitor's voltage towards the reference values determined by the

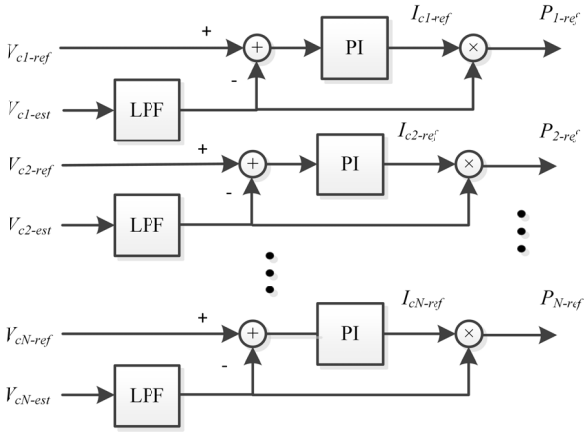

Fig. 4. Voltage controller module

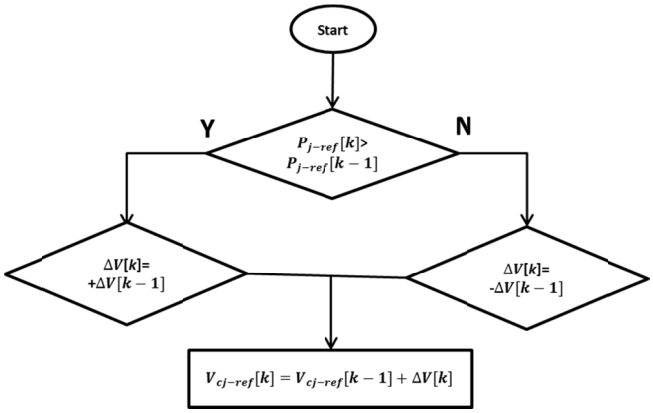

Fig. 5. MPPT module (P&O algorithm)

Perturb and Observe (P&O) algorithm implemented in the MPPT module.

The capacitors' voltages are governed by (4), which is obtained by applying Kirchhoff's current law to N dc nodes at the dc-side and assuming that the losses are negligible.

$$I_{PV-j} - C\frac{dV_{cj}}{dt} - \frac{v_j}{V_{cj}}i_g = 0 \quad , \quad (j = 1,\cdots,N), \tag{4}$$

where C represents the capacitance of the capacitors ($C=C_1=C_2=\ldots=C_N$), V_{cj} is the voltage across the individual capacitors and $I_{PV\text{-}j}$ represents the current generated by the PV array connected to the jth H-bridge.

The estimated capacitors' voltages by the CVEM enter a low pass filter to remove unwanted second order harmonic ripple. The bandwidth of the PI voltage controllers, f_v, has to meet two constraints: $f_v<0.2f_g$ and $f_v<0.1f_i$, where f_g is the grid frequency and f_i is the bandwidth of the PI current controllers. The first constraint ensures that the PI voltage controllers are not affected by the oscillating component of the inverter ac power. The second constraint makes the outer voltage controller loops at least 10 times slower than the inner current controller loop. The output of the jth PI voltage controller, $I_{cj\text{-}ref}$, corresponds to the current generated by the PV array connected to the jth H-bridge, $I_{PV\text{-}j}$. Hence, to generate the jth reference power signal, $P_{j\text{-}ref}$, the output of the jth PI controller is multiplied by the jth estimated capacitor voltage, $V_{cj\text{-}est}$. When the jth PI controller reaches the steady state, $P_{j\text{-}ref}$ is equal to the actual power generated by the jth PV array, P_j. $P_{j\text{-}ref}$ is then used by the P&O algorithm implemented in the MPPT module to generate the jth reference capacitor voltage $V_{cj\text{-}ref}$. The P&O algorithm has to operate much slower than the voltage control loop, hence, the MPPT module's update frequency, f_m, is constrained to $f_m<0.1f_v$.

B. Current controller module

Block diagram of the current controller module is shown in Fig. 6 [26]. The grid current is governed by (5), which is obtained by applying Kirchhoff's voltage law to the ac side.

$$\sum_{j=1}^{N} v_j - v_g - Ri_g - L\frac{di_g}{dt} = 0, \quad (j = 1,\cdots,N), \tag{5}$$

where v_j is the output voltage generated by the jth H-bridge, L represents the inductance of the filtering inductor and R is its series resistance. v_g and i_g are the grid voltage and current respectively.

The current controller module controls the grid current in the d-q reference frame. As the system is single-phase the required quadrature signal of the grid current is generated by a quarter of a period delay function. The active power reference current, $I_{d\text{-}ref}$, is calculated as

$$I_{d-ref} = \left(\sum_{j=1}^{N} P_{j-ref} + RI_g^2\right)/V_g \tag{6}$$

where I_g and V_g are the rms values of the grid current and voltage, respectively.

The reactive power reference current, $I_{q\text{-}ref}$, is set to zero.

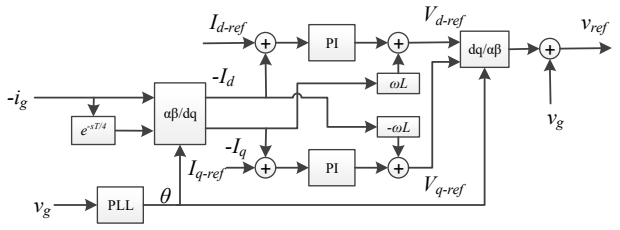

Fig. 6. Current controller module

The bandwidth of the PI current controllers, f_i, has to meet the constraint: $f_i<0.2f_s$ (where f_s is the switching frequency). The outputs of the PI current controllers are the inverter's reference ac voltage d-q components. The d-q components are then transformed back to the fixed reference frame to form the v_{ref}.

C. Power sharing module

The objective of this module is to distribute the reference voltage v_{ref} generated by the current controller among the H-bridges based on the reference powers P_{j-ref} from the voltage controller module. The module initially distributes the reference voltage among the H-Bridges equally. Therefore, the active power that each H-bridge draws is

$$P_m = \frac{\sum_{j=1}^{N} P_{j-ref}}{N} \tag{7}$$

To adjust the active power drawn by the jth H-bridge to its reference value, $P_{j\text{-}ref}$, the module modifies the reference voltage of the jth H-bridge, $v_{j\text{-}ref}$, as

$$v_{j-ref} = \frac{v_{ref}}{N} + \frac{P_{j-ref} - P_m}{I_g}\frac{i_g}{I_g} \quad , \quad (j = 1,\ldots,N) \tag{8}$$

As it can be seen from (8), the modified reference voltages of the individual H-bridges do not alter the total ac voltage reference of the inverter.

The converter has to be designed with sufficient margin to be able to operate under various environmental conditions. Therefore, to ensure proper operation of the power sharing module, a possible maximum and minimum power mismatch has to be calculated. The possible mismatch can be calculated from the PS-PWM switching technique criterion, which requires that the inverter reference voltage has to remain lower than the capacitor voltage in order to avoid overmodulation. Therefore, in the worst case scenario (when the capacitor voltage is minimum)

$$\left|V_{c-j-\min}\right| = \left|\frac{v_{ref}}{N} + \frac{P_{j-ref} - P_m}{I_g}\frac{i_g}{I_g}\right| \quad , \quad (j = 1,\ldots,N) \tag{9}$$

where $V_{c\text{-}j\text{-}min}$ is the minimum value that the oscillating jth capacitor voltage reaches. Neglecting the filter inductor's resistance and assuming that the grid current is in phase with the grid voltage, (9) can be rewritten as

This article has been accepted for publication in a future issue of this journal, but has not been fully edited. Content may change prior to final publication. Citation information: DOI 10.1109/TIE.2016.2544243, IEEE Transactions on Industrial Electronics

$$\left|V_{c-j-\min}\right| = \left|\frac{\sqrt{2}(V_g + jXI_g)}{N} + \frac{\Delta P_{j-\max}}{I_g}\frac{\sqrt{2}I_g}{I_g}\right| \quad (10)$$
$$, \quad (j = 1,\ldots,N).$$

In (10), X represents the reactance of L and $\Delta P_{j\text{-}max}$ is the maximum possible power mismatch. Replacing I_g with NP_m/V_g yields

$$\left|V_{c-j-\min}\right| = \sqrt{2}\left|\frac{V_g^2 + jXNP_m}{NV_g} + \frac{V_g \Delta P_{j-\max}}{NP_m}\right| \quad (11)$$
$$, \quad (j = 1,\ldots,N).$$

From (11),

$$\Delta P_{j-\max} = P_m\left(\frac{N}{V_g}\sqrt{\frac{V_{c-j-\min}^2}{2} - \frac{X^2P_m^2}{V_g^2}} - 1\right) \quad (12)$$
$$, \quad (j = 1,\ldots,N).$$

The minimum possible power mismatch, $\Delta P_{j\text{-}min}$, for the jth H-bridge can be determined from the maximum power mismatch limits of the other H-bridges as

$$\Delta P_{j-\min} = \sum_{k\neq j} \Delta P_{k-\max}, \quad (j = 1,\ldots,N). \quad (13)$$

D. Switching Module

In the switching module, the estimated capacitors' voltages' ripples are used for feedforward modification of the reference ac voltage signals [27], [28]. As a result, variations in the capacitors' voltages have minimal effect on the inverter ac voltages and current.

The PS-PWM technique is utilized to generate the switching signals for each H-bridge. Using the PS-PWM switching technique, the switching frequency of each module remains constant, which in theory results in sampling of the estimated capacitor' voltages at twice the switching frequency of each H-bridge. However, in practice, measurement of the output voltage at narrow pulses is difficult, less accurate and requires fast Analogue to Digital Converter (ADC) modules. This issue can be resolved either by ignoring the narrow pulses in the CVEM or by removing/limiting the width of the narrow pulses in the switching module. In this paper, the first approach is used, as modifying the generated output voltage would adversely affect the current Total Harmonics Distortion (THD) and increase the PWM module implementation complexity. Since the occurrence of pulses that are narrower than a minimal pulse width is infrequent, ignoring these pulses does not have any significant effect on the operation of the control system.

V. Simulation Results

A PV array connected to the grid through a 9-level CHB converter is used to simulate the operation of the proposed dc-side sensorless system. The PV array is composed of four subarrays and each subarray has two series connected REC220AE-US PV modules. The model of the REC220AE-US PV module and its parameters can be found in [29], [30]. Each subarray feeds one H-bridge. The parameters of the simulated system are given in Table I.

TABLE I
Parameters of the Simulated System

Symbol	Quantity	Value
$V_{g\text{-}rms}$	Grid voltage *rms* value	110 V
C	H-bridge DC capacitance	3.3×10^{-3} F
L	Filter inductance	2 mH
f_s	Switching frequency (per H-Bridge)	1600 Hz
f_g	Grid frequency	50 Hz
S	Converter nominal power	1.8 kVAr
R	Filter inductor series resistance	0.2 Ω
f_v	Bandwidth of the voltage controller	10 Hz
f_i	Bandwidth of the current controller	200 Hz
f_m	MPPT update frequency	1 Hz
N	Number of H-bridges	4

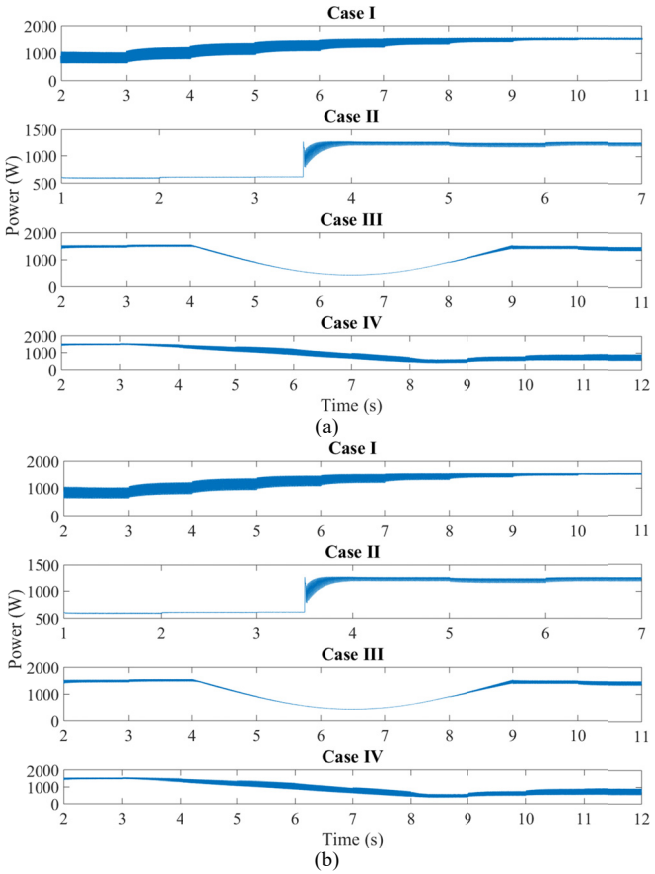

Fig. 7. a) Output power of the proposed PV system. b) Output power of a conventional system with one dc voltage and one dc current sensor per H-bridge. Case I: startup test, Case II: Step irradiance change from 400 to 800 W/m^2 at t=3.5 s, Case III: Gradual irradiance change, Case IV: Gradual temperature change.

The objective of the simulations presented in this section is to demonstrate that operation of the proposed dc-side sensorless control system is comparable to a conventional system with one dc voltage and one dc current sensor per H-bridge. The results of the extracted power for both the conventional and proposed systems for four different cases are

This article has been accepted for publication in a future issue of this journal, but has not been fully edited. Content may change prior to final publication. Citation information: DOI 10.1109/TIE.2016.2544243, IEEE Transactions on Industrial Electronics

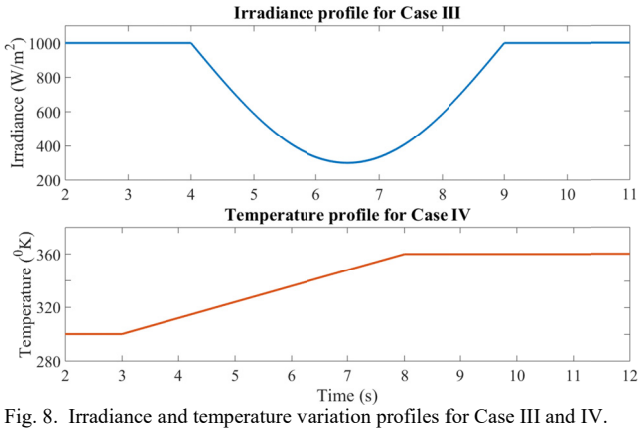

Fig. 8. Irradiance and temperature variation profiles for Case III and IV.

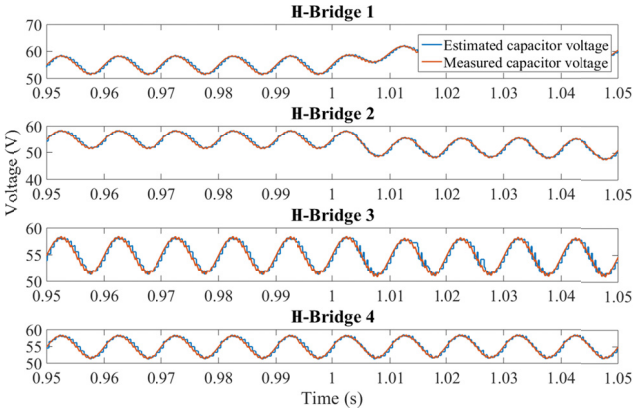

Fig. 9. Comparison of the estimated and measured capacitors' voltages.

compared in Fig. 7. Case I represents a startup test in which the reference for each capacitor voltage is fixed to 65 V before activation of the MPPT module at t=2 s. A step change in the PV array irradiance level from 400 to 800 W/m^2 is simulated in Case II. In Case III, the PV array irradiance changes gradually as shown in Fig. 8 (temperature remains constant at 300 ^{0}K). Finally, in Case IV, the PV array is subjected to temperature variation at a constant 1000 W/m^2 irradiance level as shown in Fig. 8.

As it can be concluded in Fig. 7, the performance of the proposed PV system closely matches the conventional one in all of the conducted simulation case studies. This demonstrates that the outer control loops of the control system that operate at low frequency (voltage control loop and the MPPT) are unaffected as the CVEM is able to update the capacitors' voltages with much faster frequency.

Operation of the CVEM is demonstrated in Fig. 9. Initially, all capacitors voltages are fixed to 55 V. Then, at time t=1 s the reference capacitor voltages of the H-Bridge 1 and 2 are changed to 65 V and 50 V, respectively. As it can be seen from the results, the CVEM is able to follow the actual voltages closely even during the transients.

VI. Experimental Results

To experimentally validate the proposed control system, a 7-level CHB multilevel converter was constructed by a series connection of three POWEREX PP75B060 H-bridges. Terrasas 600 PV simulators were used to simulate three series

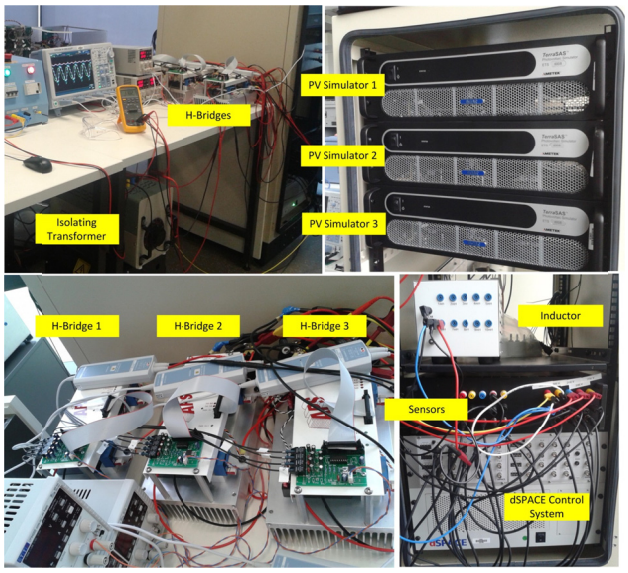

Fig. 10. Experimental setup

TABLE II
Parameters of the Experimental Setup

Symbol	Quantity	Value
$V_{g\text{-}rms}$	Grid voltage *rms* value	110 V
C	H-bridge dc capacitance	3.3×10^{-3} F
L	Filter inductance	6 mH
f_s	Switching frequency (per H-bridge)	800 Hz
f_g	Grid frequency	50 Hz
S	Converter nominal power	2 kVAr
R	Filter inductor series resistance	0.2 Ω
f_v	Bandwidth of the voltage controller	10 Hz
f_i	Bandwidth of the current controller	100 Hz
f_m	MPPT update frequency	1 Hz
N	Number of H-bridges	3

connected REC220AE-US PV modules connected to each H-bridge. The control system was implemented on dSPACE DS1006 processor board and the feedback signals were measured using a DS2004 ADC module. The experimental setup is shown in Fig. 10 and its parameters are given in Table II. In the following experiments, the output voltage pulses narrower than 40 μs were disregarded by the capacitors voltage estimation module.

Operation of the proposed dc-side sensorless CHB multilevel converter based PV control system with nominal power is demonstrated in Figs. 11-13. During the experiment, the irradiance and the temperature were set in the PV simulators to 1000 W/m^2 and 25^{0}C respectively.

Fig. 11 compares the capacitors voltages estimated by the capacitors' voltages estimation module with the actual measured values. As it can be seen the module is able to track the actual measured voltage with adequate accuracy and resolution.

Fig. 12 shows the capacitors voltages, the grid current, the grid voltage and the ac-side voltage of the inverter while delivering the nominal power with unity power factor to the grid. Fig. 13 shows the Fast Fourier Transform analysis of the injected grid current while delivering the nominal power with

This article has been accepted for publication in a future issue of this journal, but has not been fully edited. Content may change prior to final publication. Citation information: DOI 10.1109/TIE.2016.2544243, IEEE Transactions on Industrial Electronics

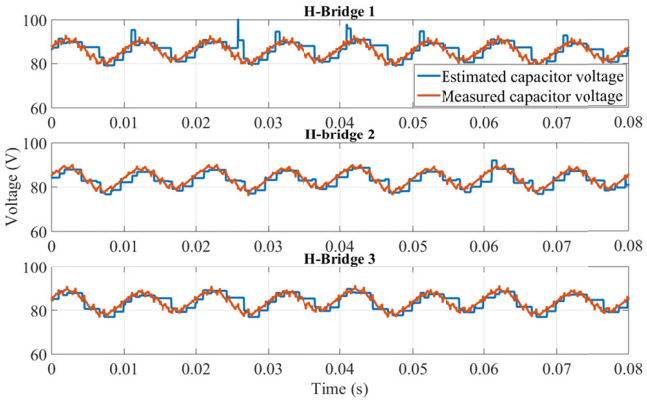

Fig. 11. Comparison of the estimated and measured capacitors' voltages.

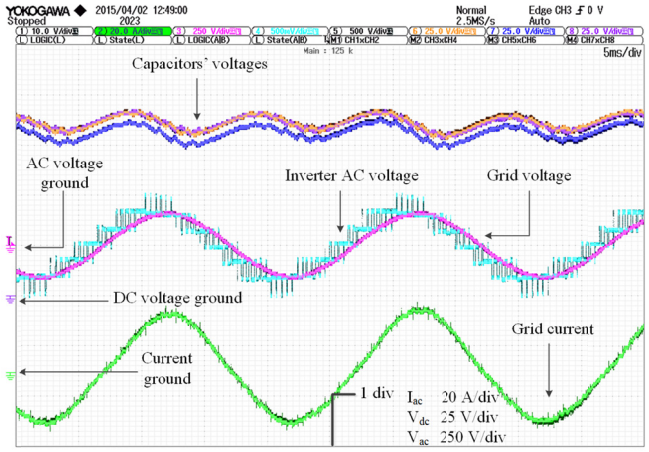

Fig. 12. The capacitors' voltages, the grid current, the voltage and the inverter ac side voltage while delivering the nominal power with unity power factor to the grid.

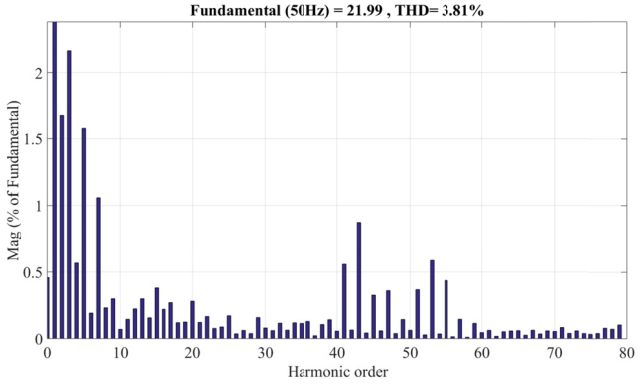

Fig. 13. Fast Fourier Transform analysis of the injected grid current while delivering the nominal power with unity power factor to the grid.

unity power factor to the grid. The current THD is less than 5%.

In the next experiment, the irradiance level in PV simulator 1 which is connected to H-Bridge 1 was programmed to follow the pattern shown in Fig. 14. The irradiance in the remaining two PV simulators was fixed to 450 W/m^2. The performance of the proposed system was compared with the conventional system which uses both the dc current and the dc voltage sensors for each H-bridge.

The output current of PV simulator 1 for both systems are

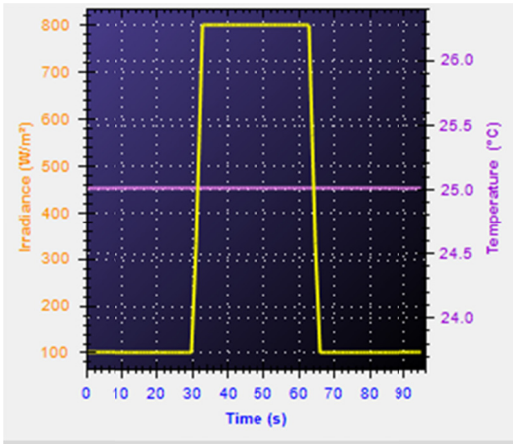

Fig. 14. Irradiance level pattern programmed in the PV simulator 1.

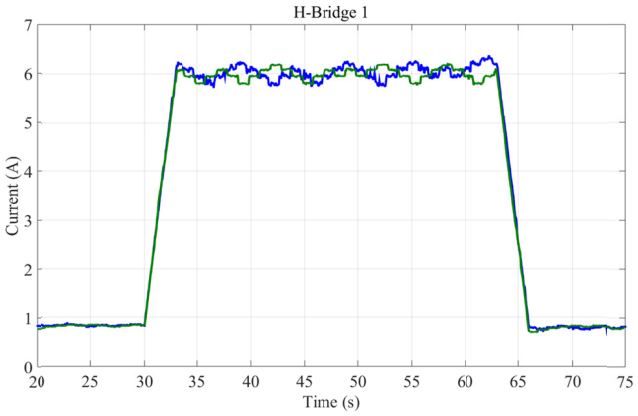

Fig. 15. Comparison of the output current of PV simulator 1 for the proposed and conventional systems.

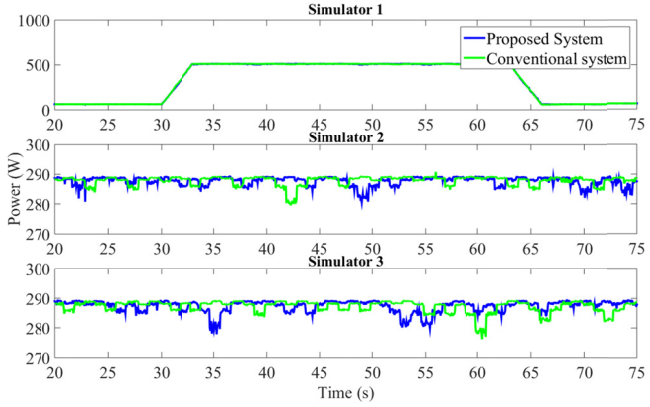

Fig. 16. Comparison of the PV simulators' output powers for the proposed and conventional systems.

shown in Fig. 15.

Fig. 16 compares the PV simulators' output powers. As it can be seen, the transient response of the proposed dc-side sensorless system is comparable with the conventional system.

To show that the proposed system is able to operate under unbalanced conditions without degradation in performance when compared to the conventional one, the MPPT performance accuracy (percentage of the power extracted from the maximum available PV power) is compared in Fig. 17.

Furthermore, a comparison of the total power and energy extracted from the PV simulators by both the proposed and

This article has been accepted for publication in a future issue of this journal, but has not been fully edited. Content may change prior to final publication. Citation information: DOI 10.1109/TIE.2016.2544243, IEEE Transactions on Industrial Electronics

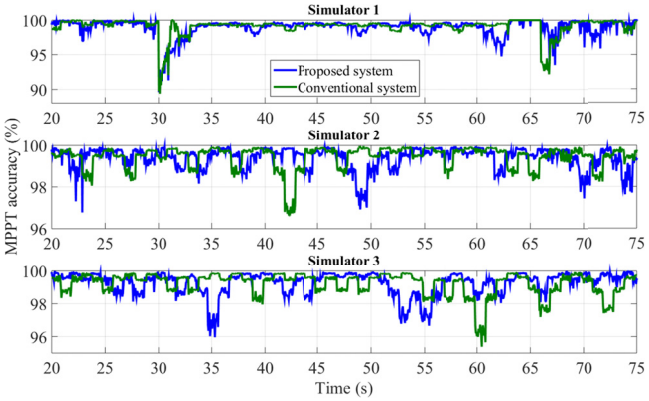

Fig. 17. Comparison of the MPPT performance accuracy for the proposed and conventional systems.

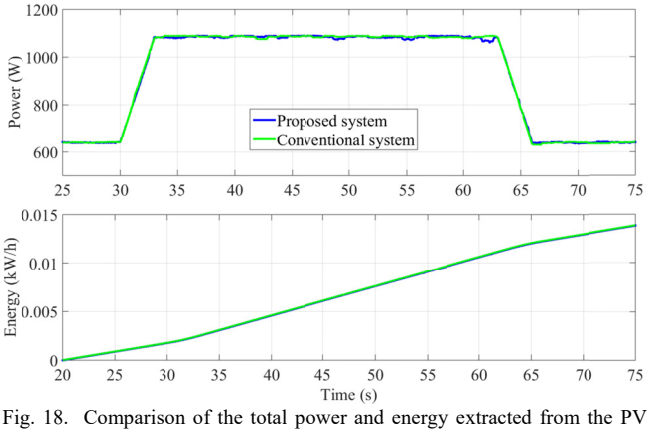

Fig. 18. Comparison of the total power and energy extracted from the PV simulators by the proposed and conventional systems.

conventional systems is depicted in Fig. 18. This data demonstrates that the performance of the proposed system does not deteriorate when the dc-side sensors are eliminated.

It is worthwhile to mention that even though the instantaneous powers generated by each H-bridge do not match, the average total generated power remains almost the same for both system as demonstrated in Fig. 18.

VII. Conclusion

A dc-side sensorless CHB multilevel converter based PV system has been proposed and experimentally verified. Experimental tests on a 7-level CHB multilevel converter based PV system showed that performance of the proposed system was comparable with a conventional system that employed all dc-side sensors. The main benefits of eliminating the dc side sensors are reduced cost, simpler hardware and increased reliability of the PV system. The operation of the proposed control system under the switching devices failure has not been addressed in this work and needs to be studied in detail in the future to improve reliability of the system.

References

[1] O. Alonso, P. Sanchis, E. Gubia, and L. Marroyo, "Cascaded H-bridge multilevel converter for grid connected photovoltaic generators with independent maximum power point tracking of each solar array," in *Proc. IEEE PESC*, vol.2, pp. 731-735, 2003.

[2] E. Villanueva, P. Correa, J. Rodriguez, and M. Pacas, "Control of a Single-Phase Cascaded H-Bridge Multilevel Inverter for Grid-Connected Photovoltaic Systems," *IEEE Trans. Ind. Electron.,* vol. 56, pp. 4399-4406, 2009.

[3] S. Kouro, W. Bin, A. Moya, E. Villanueva, P. Correa, and J. Rodriguez, "Control of a cascaded H-bridge multilevel converter for grid connection of photovoltaic systems," in *Proc. IEEE IECON*, pp. 3976-3982, 2009.

[4] C. Cecati, F. Ciancetta, and P. Siano, "A Multilevel Inverter for Photovoltaic Systems With Fuzzy Logic Control," *IEEE Trans. Ind. Electron.,* vol. 57, pp. 4115-4125, 2010.

[5] J. J. Negroni, D. Biel, F. Guinjoan, and C. Meza, "Energy-balance and sliding mode control strategies of a cascade H-bridge multilevel converter for grid-connected PV systems," in *Proc. IEEE ICIT*, pp. 1155-1160, 2010.

[6] M. Chithra and S. G. B. Dasan, "Analysis of cascaded H bridge multilevel inverters with photovoltaic arrays," in *Proc. ICETECT*, pp. 442-447, 2011.

[7] S. Rivera, S. Kouro, B. Wu, J. I. Leon, J. Rodriguez, and L. G. Franquelo, "Cascaded H-bridge multilevel converter multistring topology for large scale photovoltaic systems," in *Proc. IEEE ISIE,* pp. 1837-1844, 2011.

[8] S. Rivera, W. Bin, S. Kouro, W. Hong, and Z. Donglai, "Cascaded H-bridge multilevel converter topology and three-phase balance control for large scale photovoltaic systems," in *Proc. IEEE PEDG,* 2012, pp. 690-697, 2012.

[9] J. Chavarria, D. Biel, F. Guinjoan, C. Meza, and J. J. Negroni, "Energy-Balance Control of PV Cascaded Multilevel Grid-Connected Inverters Under Level-Shifted and Phase-Shifted PWMs," *IEEE Trans. Ind. Electron.,* vol. 60, pp. 98-111, 2013.

[10] L. Xi, G. Baoming, and P. Fang Zheng, "Minimizing dc capacitance requirement of cascadeded H-bridge multilevel inverters for photovoltaic systems by 3rd harmonic injection," in *Proc. IEEE APEC,* pp. 240-245, 2012.

[11] M. A. P. Oliveira and M. B. R. Correa, "Analysis of grid-tied single phase multilevel inverters powered by photovoltaic panels under partial shading conditions," in *Proc. IEEE PEDG,* pp. 483-486, 2012.

[12] Z. Wei, C. Hyuntae, G. Konstantinou, M. Ciobotaru, and V. G. Agelidis, "Cascaded H-bridge multilevel converter for large-scale PV grid-integration with isolated dc-dc stage," in *Proc. IEEE PEDG,* pp. 849-856, 2012.

[13] X. Bailu, S. Ke, M. Jun, F. Filho, and L. M. Tolbert, "Control of cascaded H-bridge multilevel inverter with individual MPPT for grid-connected photovoltaic generators," in *Proc. IEEE ECCE,* pp. 3715-3721, 2012.

[14] F. Wu, B. Sun, J. Duan, and K. Zhao, "On-Line Variable Topology-Type Photovoltaic Grid-Connected Inverter," *IEEE Trans. Ind. Electron.,* vol. PP, pp. 1-1, 2015.

[15] Y. Liu, B. Ge, H. Abu-Rub and F. Z. Peng, "An Effective Control Method for Three-Phase Quasi-Z-Source Cascaded Multilevel Inverter Based Grid-Tie Photovoltaic Power System," *IEEE Tran. Ind. Electron.,* vol. 61, pp. 6794-6802, 2014.

[16] D. Sun, B. Ge; X. Yan; D. Bi; H. Zhang; Y. Liu; H. Abu-Rub; L. Ben-Brahim; and F. Z. Peng, "Modeling, Impedance Design, and Efficiency Analysis of Quasi-Z-Source Module in Cascaded Multilevel Photovoltaic Power System," *IEEE Trans. Ind. Electron.,* vol. 61, pp. 6108-6117, 2014.

[17] Y. Yu, G. Konstantinou, B. Hredzak and V. G. Agelidis, "Operation of Cascaded H-Bridge Multilevel Converters for Large-Scale Photovoltaic Power Plants Under Bridge Failures," *IEEE Trans. Ind. Electron.*, vol. 62, no. 11, pp. 7228-7236, Nov. 2015.

[18] J. Yuncong, J. A. A. Qahouq, and T. A. Haskew, "Adaptive Step Size With Adaptive-Perturbation-Frequency Digital MPPT Controller for a Single-Sensor Photovoltaic Solar System," *IEEE Trans. Power Electron.,* vol. 28, pp. 3195-3205, 2013.

[19] E. S. Sreeraj, K. Chatterjee, and S. Bandyopadhyay, "One-Cycle-Controlled Single-Stage Single-Phase Voltage-Sensorless Grid-Connected PV System," *IEEE Trans. Ind. Electron.,* vol. 60, pp. 1216-1224, 2013.

[20] E. Dallago, D. G. Finarelli, U. P. Gianazza, A. L. Barnabei, and A. Liberale, "Theoretical and Experimental Analysis of an MPP Detection Algorithm Employing a Single-Voltage Sensor Only and a Noisy Signal," *IEEE Trans. Power Electron.,* vol. 28, pp. 5088-5097, 2013.

[21] E. Dallago, A. Liberale, D. Miotti, and G. Venchi, "Direct MPPT algorithm for PV sources with only voltage measurements," *IEEE Trans. Power Electron.,* vol. PP, pp. 1-1, 2015.

[22] L. Yidan and W. Bin, "A Novel DC Voltage Detection Technique in the CHB Inverter-Based STATCOM," *IEEE Trans. Power Del.,* vol. 23, pp. 1613-1619, 2008.
[23] G. Farivar, V. G. Agelidis, and B. Hredzak, "A generalized capacitors voltage estimation scheme for multilevel converters," in *Proc. EPE*, pp. 1-5, 2014.
[24] J. de Leon Morales, M. F. Escalante, and M. T. Mata-Jimenez, "Observer for DC voltages in a cascaded H-bridge multilevel STATCOM," *IET Electric Power Appl.,* vol. 1, pp. 879-889, 2007.
[25] M. C. Cavalcanti, G. M. S. Azevedo, B. A. Amaral, K. C. de Oliveira, F. A. S. Neves, and Z. D. Lins, "Efficiency Evaluation in Grid Connected Photovoltaic Energy Conversion Systems," in *Proc. IEEE PESC*, pp. 269-275, 2005.
[26] G. Farivar, B. Hredzak and V. G. Agelidis, "Decoupled Control System for Cascaded H-Bridge Multilevel Converter Based STATCOM," in *IEEE Trans. Ind. Electron.*, vol. 63, no. 1, pp. 322-331, Jan. 2016.
[27] S. Kouro, P. Lezana, M. Angulo, and J. Rodriguez, "Multicarrier PWM With DC-Link Ripple Feedforward Compensation for Multilevel Inverters," *IEEE Trans. Power Electron.,* vol. 23, pp. 52-59, 2008.
[28] G. Farivar, B. Hredzak and V. G. Agelidis, "Reduced-Capacitance Thin-Film H-Bridge Multilevel STATCOM Control Utilizing an Analytic Filtering Scheme," *IEEE Trans. Ind. Electron.*, vol. 62, no. 10, pp. 6457-6468, Oct. 2015.
[29] G. Farivar and B. Asaei, "A New Approach for Solar Module Temperature Estimation Using the Simple Diode Model," *IEEE Trans. Energy Convers.,* vol. 26, pp. 1118-1126, 2011.
[30] G. Farivar, B. Asaei, and S. Mehrnami, "An Analytical Solution for Tracking Photovoltaic Module MPP," *IEEE J. Photovolt.,* vol. 3, pp. 1053-1061, 2013.

Ghias Farivar (S'13) received the B.Sc. degree in electrical engineering from Nooshirvani Institute of Technology, Babol, Iran, in 2008 and the M.Sc degree in power electronics from the University of Tehran, Tehran, Iran in 2011.
He is currently a PhD student at the Australian Energy Research Institute, University of New South Wales (UNSW), Sydney, Australia.
His research interests include renewable energy systems, power convertors, FACTS devices, and hybrid electric vehicles.

Branislav Hredzak (M'98-SM'13) received the B.Sc./M.Sc. degree from the Technical University of Kosice, Slovak Republic, in 1993 and the Ph.D. degree from Napier University of Edinburgh, UK, in 1997, all in Electrical Engineering.
He was as a Lecturer and a Senior Researcher in Singapore from 1997 to 2007. He is currently a Senior Lecturer in the School of Electrical Engineering and Telecommunications, The University of New South Wales, Sydney, NSW, Australia. His current research interests include hybrid storage technologies and advanced control systems for power electronics and storage systems.

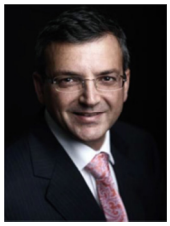

Vassilios G. Agelidis (S'89-M'91-SM'00-F'16) was born in Serres, Greece. He received the B.Eng. degree in electrical engineering from the Democritus University of Thrace, Thrace, Greece, in 1988; the M.S. degree in applied science from Concordia University, Montreal, QC, Canada, in 1992; and the Ph.D. degree in electrical engineering from Curtin University, Perth, Australia, in 1997.
He was with Curtin University (1993-1999); the University of Glasgow, Glasgow, U.K. (2000-2004); Murdoch University, Perth, Australia (2005-2006); and the University of Sydney, Sydney, Australia (2007-2010). He is currently the Director of the Australian Energy Research Institute, School of Electrical Engineering and Telecommunications, University of New South Wales (UNSW), Sydney, Australia.
Prof. Agelidis received the Advanced Research Fellowship from the U.K.'s Engineering and Physical Sciences Research Council in 2004. He was the Vice President for Operations with the IEEE Power Electronics Society (PELS) from 2006 to 2007. He was an AdCom Member of the IEEE PELS from 2007 to 2009 and the Technical Chair of the 39th IEEE Power Electronics Specialists Conference in 2008 held in Rhodes, Greece.